

A Universal Intrinsic Scale of Hole Concentration for High- T_c Cuprates

T. Honma*

Department of Physics and Texas Center for Superconductivity and Advanced Materials,
University of Houston, Houston, TX77204-5005, U.S.A. and
Department of Physics, Asahikawa Medical College, Asahikawa 078-8510, Japan

P.H. Hor,¹ and H.H. Hsieh^{1,2}

¹Department of Physics and Texas Center for Superconductivity and Advanced Materials,
University of Houston, Houston, TX77204-5005, U.S.A.

²Synchrotron Radiation Research Center, Hsinchu, Taiwan 30077, Republic of China and
Synchrotron Radiation Research Center, Hsinchu, Taiwan 30077, Republic of China

M. Tanimoto

Department of Physics, Asahikawa Medical College, Asahikawa 078-8510, Japan

(Dated: January 28, 2020)

We have measured room-temperature thermoelectric power S^{290} as a function of hole concentration per CuO₂ layer, P_{pl} in $Y_{1-x}Ca_xBa_2Cu_3O_6$ ($P_{pl} = x/2$) with no oxygen in the Cu-O chain layer. $S^{290}(P_{pl})$, the room-temperature TEP as a function of P_{pl} , of $Y_{1-x}Ca_xBa_2Cu_3O_6$ behaves identically to that of $La_{2-z}Sr_zCuO_4$ ($P_{pl} = z$). We argue that $S^{290}(P_{pl})$ represents a measure of the intrinsic equilibrium electronic states of doped holes and, therefore, can be used as a common scale for the carrier concentrations of layered cuprates. We show that the P_{pl} determined by the new scale is consistent with both microscopic hole concentration determined by NQR and the macroscopic one determined by the formal valency of Cu. On the basis of $S^{290}(P_{pl})$, we uncover a universal phase diagram in which all the experimentally determined pseudogap temperatures fall on two common curves, upper and lower pseudogaps. We find that while pseudogaps are intrinsic properties of doped holes of a single CuO₂ layer for all high- T_c cuprates, T_c depends on the number of layers, therefore the inter-layer coupling, in each individual system.

PACS numbers: 74.25.Fy, 74.25.Dw, 74.62.Dh, 74.72.-h

I. INTRODUCTION

Understanding some of the peculiar properties of the high temperature superconductors (HTSC's) is one of the challenging problems in the condensed matter physics. Especially, in the underdoped regime, not only the unusually high superconducting transition temperature (T_c) but also many normal state properties have defied our current knowledge of metal. Over the past 17 years tremendous experimental results have been accumulated. Unfortunately, due to both the experimental and material constraints, many high quality data were collected on different materials. For instance, neutron scattering experiments require very large single crystals and therefore have almost exclusively been done on $YBa_2Cu_3O_y$ (Y123) and $La_{2-z}Sr_zCuO_4$ (LS214) that big crystals can be grown. The angle-resolved photoemission spectroscopy (ARPES), which are sensitive to the surface conditions, has been performed mainly on $Bi_2Sr_2CaCu_2O_y$, that it cleaves easily. On the other hand, resistivity ρ , Hall coefficient R_H and thermoelectric power (TEP) S have been measured on almost all HTSC's. It will be most fruitful if different measurements done on different materials can be compared and analyzed on a common ground, say, hole concentration per CuO₂ layer, P_{pl} . P_{pl} can be determined by Sr-content z ($P_{pl} = z$) in $La_{2-z}Sr_zCuO_4$ with only cation doping, but it is hard to determine P_{pl} unambiguously in the

other systems with anion doping. If P_{pl} can be determined by either ρ , R_H or S , then almost all the available data can be compared quantitatively and analyzed.

The underdoped HTSC is characterized by a gap-like anomaly appeared below a characteristic temperature, the so-called pseudogap temperature. The pseudogap behavior was first observed in ⁸⁹Y NMR Knight shift and in the ⁶³Cu spin-lattice relaxation rate $^{63}(T_1T)^{-1}$.¹ It also showed up as an anomaly in the ρ and R_H versus temperature curves.^{2,3} Subsequently, the pseudogap behavior has been observed in many experimental probes, such as ARPES,⁴ TEP,⁵ specific heat,^{6,7} time resolved quasiparticle relaxation (QPR) measurement⁸ and so on. The pseudogap temperature systematically varies with cation or anion doping in individual systems. However, due to the above reason, these pseudogap temperatures can not be compared on a common physical ground such as the hole concentration. In such a situation, the room temperature TEP (S^{290}) was proposed to be useful for determining P_{pl} .⁹ According to this scale, the pseudogap behavior is summarized on the phase diagram that the pseudogap temperature falls from higher temperature at lower hole concentration to zero at a critical hole concentration across the T_c curve.¹⁰ On the other hand, the result of ARPES suggests that the pseudogap temperature does not cross the T_c curve, but smoothly merges with T_c on the slightly overdoped side.⁴

For LS214 system where T_c appears at $P_{pl} \approx 0.06$,

passes a maximum T_c (T_c^{max}) at $P_{pl} \approx 0.16$, and finally falls to zero at $P_{pl} \approx 0.27$. It was approximated by a parabolic curve¹¹

$$T_c/T_c^{max} = 1 - 82.6(P_{pl} - 0.16)^2. \quad (1)$$

Although Formula (1) has been used with some success to estimate P_{pl} for the systems with similar parabolic variation of T_c , it cannot be used for the systems with a complex variation of T_c such as Y123. P_{pl} of Y123 was estimated from the bond valence sum (BVS) analysis, which relied on accurate knowledge of interatomic bond lengths.¹² Later, it was shown that, for some HTSC's, S^{290} can be used to estimate P_{pl} consistent with that determined by either Formula (1) or BVS analysis.⁹ The following empirical formula has been proposed.¹³

$$S^{290}[\mu V/K] = \begin{cases} 372 \exp(-32.4P_{pl}) & (0.00 < P_{pl} < 0.05) \\ 992 \exp(-38.1P_{pl}) & (0.05 < P_{pl} < 0.155) \\ 24.2 - 139P_{pl} & (0.155 < P_{pl}) \end{cases} \quad (2)$$

Formula (2) has been widely used with the distinct advantages that S^{290} is material independent. Therefore it can be used to compare physical properties as a function of P_{pl} of very different HTSC's. But, there are still difficulties in using Formula (2). For instance, there is no reason why the optimal P_{pl} , where T_c^{max} appears, should be universally ~ 0.16 for HTSC as has already been questioned in Ref. 14. It is also not trivial to apply BVS to determine P_{pl} for systems with internal strain due to the CuO chain structure such as Y123.¹⁵ Furthermore it is reported that, for LS214,⁹ $(\text{Ca}_x\text{La}_{1-x})(\text{Ba}_{1.75-x}\text{La}_{0.25+x})\text{Cu}_3\text{O}_y$ (C_xLBLC),¹⁶ and $\text{Bi}_2\text{Sr}_{2-x}\text{La}_x\text{CuO}_y$ ($\text{Bi}2201$),¹⁷ P_{pl} 's determined by Formula (1) are not consistent with those determined by Formula (2).

$\text{Y}_{1-x}\text{Ca}_x\text{Ba}_2\text{Cu}_3\text{O}_6$ (YC1236) without CuO chain has two equivalent CuO₂ planes, therefore the P_{pl} can be determined unambiguously by Ca-content x as $P_{pl} = x/2$. Following the well known approach using the empirical correlation between S^{290} and P_{pl} ,⁹ we find that $S^{290}(P_{pl})$ for YC1236 behaves identically to that for LS214. Since the crystal structure for YC1236 is very different from that for LS214, we argue that this new correlation of S^{290} can be used as an intrinsic scale of P_{pl} for different HTSC cuprates. We demonstrate that this conjecture seems to work by uncovering a universal phase diagram of the pseudogap and superconductivity. We find that while the pseudogap phase is an intrinsic property to single CuO₂ layer, the bulk T_c is governed exclusively by the inter-layer coupling.

II. EXPERIMENTAL

$\text{Y}_{1-x}\text{Ca}_x\text{Ba}_2\text{Cu}_3\text{O}_6$ with different Ca-contents of $x = 0.05, 0.10, 0.13, 0.15, 0.17, 0.18, 0.19, 0.20$, and 0.22 were prepared by causing a solid-state reaction in a proportioned mixture of Y_2O_3 (5N), CaCO_3 (5N), BaCO_3 (5N),

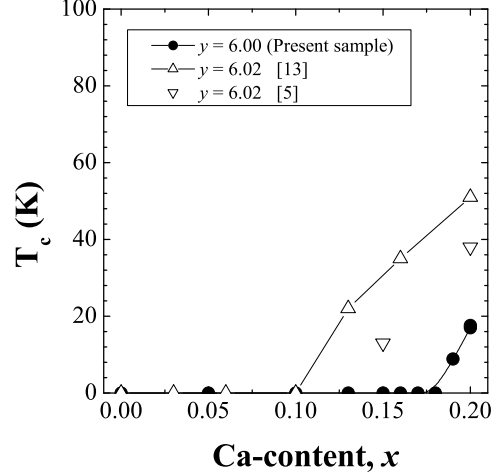


FIG. 1: Superconducting transition temperature (T_c) as a function of Ca doping level for the double-layer $\text{Y}_{1-x}\text{Ca}_x\text{Ba}_2\text{Cu}_3\text{O}_y$. The data for the samples with $y = 6.00$ and 6.02 are present work. The others are data reported in the literature.^{5,13} The solid lines are guide to the eyes.

and CuO (4N). These powders were ground, pressed and fired in flowing O_2 at 900°C for 6 h. This process was repeated several times. For the final firing, two pellets with ~ 0.5 g each were fired for $10 \sim 15$ h in flowing O_2 at $930 \sim 940^\circ\text{C}$. The O_2 gas was exchanged into Ar (99.9995 %) at the high temperature, before in the furnace with flowing Ar the samples were annealed at 750°C and cooled to room temperature. The oxygen content y was confirmed to be 6.00 ± 0.01 by using an iodometric titration technique under Ar gas. The prepared $\text{Y}_{1-x}\text{Ca}_x\text{Ba}_2\text{Cu}_3\text{O}_6$ samples with $x \leq 0.22$ were identified as a single-phase by examining the X-ray powder diffraction pattern. The $\text{Y}_{0.75}\text{Ca}_{0.25}\text{Ba}_2\text{Cu}_3\text{O}_6$ showed some minor second phase. The main peak of the second phase was below 1 % for the main peak of the 123 phase. The density of all prepared samples was over 80 % of the theoretical density. Figure 1 shows the Ca content dependence of T_c with previous reported results.^{5,13} The prepared samples shows no clear superconducting transition until $x = 0.18$, while the superconductivity appears above ~ 0.125 in the other group's sample with $y = 6.02$.^{5,13} Accordingly, the chain-site oxygen of the present samples is confirmed to be adequately reduced. The TEP was measured by an ac method with a low-frequency (33 mHz) heating technique.¹⁸

III. RESULTS AND DISCUSSION

A. Temperature dependence of TEP for $\text{Y}_{1-x}\text{Ca}_x\text{Ba}_2\text{Cu}_3\text{O}_6$

Figure 2 shows the typical T -dependence of TEP for a series of fully deoxygenated $\text{Y}_{1-x}\text{Ca}_x\text{Ba}_2\text{Cu}_3\text{O}_6$ with

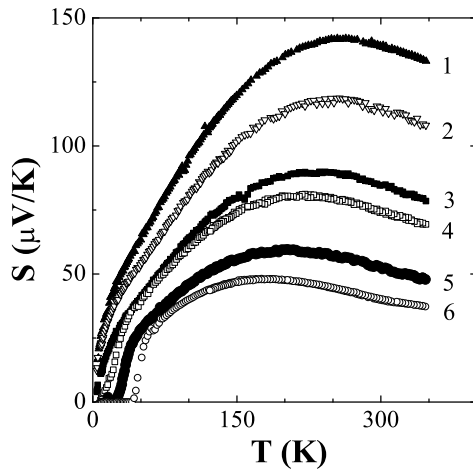


FIG. 2: The evolution of $S(T)$ for different Ca content of the double-layer $Y_{1-x}Ca_xBa_2Cu_3O_6$. The Ca-content of samples 1-6 are 0.10, 0.13, 0.15, 0.18, 0.20, and 0.22.

$0.05 \leq x \leq 0.22$. The oxygen content is fixed to be 6.00 ± 0.01 here. Typically, upon increasing T , positive S rises towards a broad peak at a temperature T_S^* and S decreases almost linearly for $T > T_S^*$. T_S^* was reported to be closely related with pseudogap temperature.⁵ The T -dependence of TEP, $S(T)$ systematically changes with Ca doping. The T_S^* becomes lower with Ca doping and the magnitude of TEP decreases. The observed $S(T)$ is very similar to that reported in LS214,^{19,20,21,22,23,24,25} $C_{0.4}LBLC$,¹⁶ and $CaLaBaCu_3O_y$ (CLBC)²⁶ without ordered CuO chain. Thus, it is confirmed that there is no feature of the presence of a significant chain contribution

to TEP.⁵

$S(T)$ can be well scaled by the value S^* and temperature T_S^* of the peak as shown in Fig. 3. S/S^* can be fitted to a $\log T$ law for $0.3 < T/T_S^* < 0.8$ as shown in the inset. We confirmed that $S(T)$ data of $Bi_2Sr_2Ca_{1-x}Y_xCu_2O_y$ (Bi2212),²⁷ CLBC,²⁶ and $C_{0.4}LBLC$ ¹⁶ also show the same scaling behavior by using the reported $S(T)$ data. $\log T$ behavior for $T < T_S^*$ was reported in CLBC²⁶ and $YBa_2Cu_3O_y$ ($y < 6.48$).⁹ Similar scaling behavior was also reported in the single layer LS214.²⁸ Since all the above observations were done on samples without ordered CuO chains like Y123, we conclude that the broad peak at T_S^* , $\log T$ dependence for $T < T_S^*$ and T linear behavior for $T > T_S^*$ are intrinsic characteristic TEP properties of doped holes in the CuO_2 layer.

B. Room temperature (RT) scale for hole concentration

Figure 4 shows S^{290} on the logarithmic scale as a function of P_{pl} . The closed circles represent the S^{290} for the full deoxygenated series $Y_{1-x}Ca_xBa_2Cu_3O_6$ with $0.05 \leq x \leq 0.22$. The P_{pl} can be determined unambiguously by Ca-content x as $P_{pl} = x/2$, since YC1236 has two equivalent CuO_2 planes without CuO chain. For the comparison, the reported results of S^{290} in LS214^{9,19,20,21,22,23,24,25} are represented by the other symbols and the universal curve proposed in Ref. 9 are also shown as the broken line. While the observed $\log(S^{290})$ of YC1236 varies linearly with P_{pl} , this does not follow the universal line. This new relation can be represented by Formula (3a). It can be clearly seen that

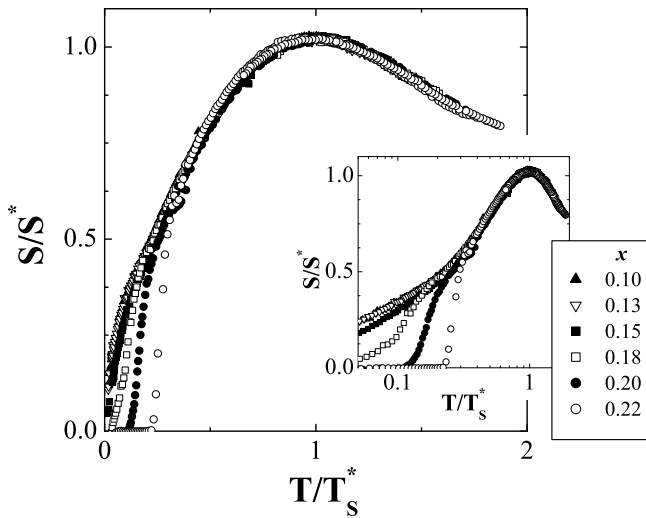


FIG. 3: S/S^* as a function of T/T_S^* for different Ca content of the double-layer $Y_{1-x}Ca_xBa_2Cu_3O_6$. The inset shows S/S^* vs T/T_S^* on the logarithmic scale.

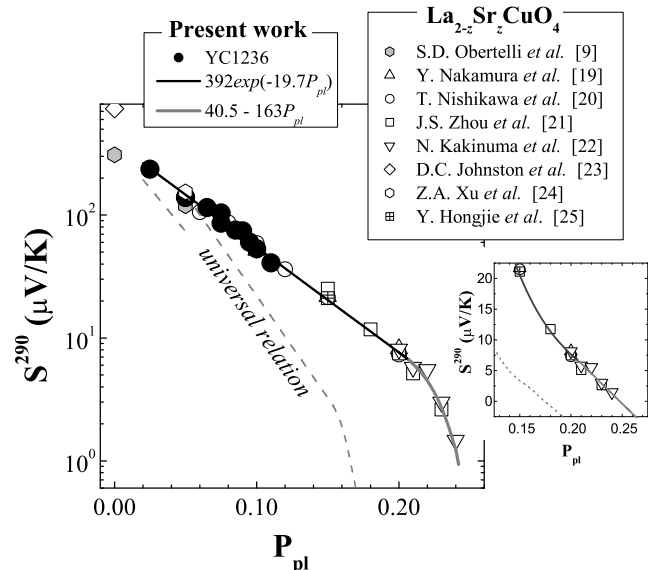


FIG. 4: S^{290} on the logarithmic scale vs P_{pl} for YC1236 and LS214. Inset: S^{290} on the linear scale vs P_{pl} . The broken line shows the universal curve proposed in Ref. 9.

S^{290} of $\text{La}_{2-z}\text{Sr}_z\text{CuO}_4$ with $0.05 \leq z \leq 0.21$ fall exactly on the same curve as $S^{290}(P_{pl})$ for YC1236. For $P_{pl} \geq 0.21$, $S^{290}(P_{pl})$ of LS214 changes from exponential to linear in P_{pl} as shown in the inset of Fig. 4. In the pure La_2CuO_4 , there is the large scattering of S^{290} as shown in Fig. 4. $S^{290}(P_{pl})$ of the double-layer YC1236 is identical to that of the single-layer LS214, in spite of the quite different and complex crystal structures, leads us to conjecture that the present relation for $S^{290}(P_{pl})$ can serve as a universal scale of P_{pl} for layered HTSC with equivalent CuO_2 layers.²⁹

$$S^{290}[\mu\text{V}/\text{K}] = \begin{cases} 392 \exp(-19.7P_{pl}) & (0.02 \leq P_{pl} \leq 0.21) \\ 40.5 - 163P_{pl} & (0.21 < P_{pl}) \end{cases} \quad (3a)$$

In Ref. 9, the $S^{290}(P_{pl})$ of $\text{La}_{2-z}\text{Sr}_z\text{CuO}_4$ did not follow Formula (2). Two possibilities were pointed out.⁹ The deviation may arise from scattering effects associated with the increasing concentration of oxygen vacancies within the CuO_2 planes which occur especially for $z > 0.12$. Structural instabilities that are related to the orthorhombic-tetragonal transition may have some effect. Since we know that YC1236 is tetragonal at room temperature³⁰ and the oxygen content is fixed at 6.00 ± 0.01 , the identical $S^{290}(P_{pl})$ behaviors for both YC1236 and LS214 has effectively ruled out both possibilities.

C. Application of RT scale to $\text{Y}_{1-x}\text{Ca}_x\text{Ba}_2\text{Cu}_3\text{O}_y$

Many TEP data for $\text{Y}_{1-x}\text{Ca}_x\text{Ba}_2\text{Cu}_3\text{O}_y$ have been reported.^{9,16,28,31,32,33,34} The anisotropy of the in-plane resistivity becomes significant when $y \gtrsim 6.68$ ($P_{pl} \gtrsim 0.18$) in $\text{YBa}_2\text{Cu}_3\text{O}_y$.² Therefore we assume that the Y123 below $y \approx 6.68$ does not have the conductive chain or chain

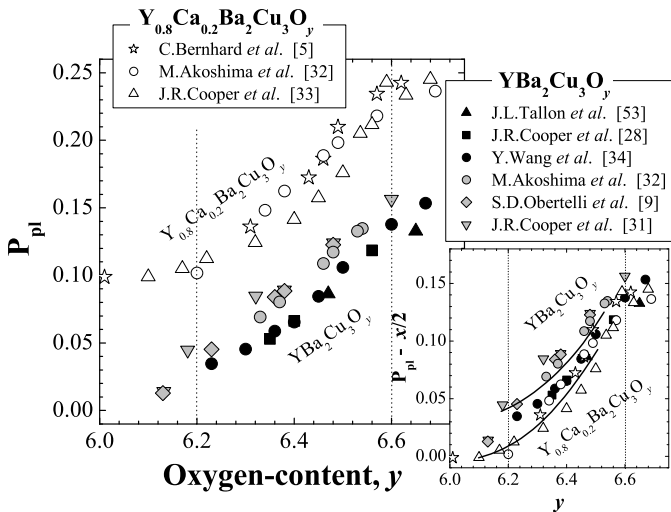


FIG. 5: P_{pl} determined from S^{290} as a function of oxygen-content, y in $\text{Y}_{1-x}\text{Ca}_x\text{Ba}_2\text{Cu}_3\text{O}_y$. The inset shows the effective hole concentration ($P_{pl} - x/2$) by the oxygen doping alone. The solid lines are guide to the eyes.

contribution to the transport property. Consequently, for the Y123 systems, the RT scale for the TEP was applied to the samples up to $y \approx 6.7$. Figure 5 shows the P_{pl} determined from S^{290} as a function of oxygen-content, y for $\text{Y}_{1-x}\text{Ca}_x\text{Ba}_2\text{Cu}_3\text{O}_y$. The P_{pl} 's for $\text{YBa}_2\text{Cu}_3\text{O}_y$ are plotted by the closed black/gray symbols. The P_{pl} 's for $\text{Y}_{0.8}\text{Ca}_{0.2}\text{Ba}_2\text{Cu}_3\text{O}_y$ are plotted by the open symbols.

In $\text{YBa}_2\text{Cu}_3\text{O}_y$, the hole carrier appears by oxygen doping beyond $y \approx 6.15$. There seems to be a threshold of the oxygen-content for generating the hole carrier. Above $y \approx 6.2$, the hole carriers increase with oxygen doping. The $P_{pl}(y)$ curve tends to divide into two curves in the range of $6.2 < y < 6.6$. The split $P_{pl}(y)$ curve may be related to the formation of the CuO chain structure or the inhomogeneity of oxygen distribution on the CuO chain site. The Ca-doped Y123 shows a slight different behavior of $P_{pl}(y)$ for Y123. In $\text{Y}_{0.8}\text{Ca}_{0.2}\text{Ba}_2\text{Cu}_3\text{O}_y$, until $y \approx 6.2$, the P_{pl} is almost 0.10, equal to the hole concentration generated by Ca doping of 0.20. This suggests the hole carriers are generated through the Ca doping. Above $y \approx 6.2$, the hole carriers significantly increase with oxygen doping. This is due to the generation of the hole carriers by oxygen doping. But, there is no threshold behavior due to Ca-doping. The $P_{pl}(y)$ curve tends to divide into two curves like Y123. In YC1236, the hole carrier can be generated even by slight Ca doping as shown in Fig. 4. The creation of hole carrier by oxygen doping may need the adequate oxygen content or threshold of hole carrier. The inset of Fig. 5 shows the effective hole concentration ($P_{pl} - x/2$) due to oxygen doping alone. Although there is some scattering, the generation of hole carrier by oxygen doping is found to be slight suppressed in the Ca-doped samples. The orthorhombic-tetragonal transition occurs in the range of $6.3 \lesssim y \lesssim 6.5$.³² The Ca doping may influence the formation of the microscopic CuO chain ordering. In the CLBCO and C_xLBLCO with significant Ca doping, there is no ordered CuO chain like Y123.⁵

Figure 6 shows the T_c as a function of P_{pl} for $\text{Y}_{1-x}\text{Ca}_x\text{Ba}_2\text{Cu}_3\text{O}_y$. There are two T_c vs P_{pl} curves. One is that the T_c appears at $P_{pl} \approx 0.09$ and above ~ 0.1 is proportional to P_{pl} (curve A). The other is that the T_c appears at $P_{pl} \approx 0.05$ and around ~ 0.18 merges into the curve A (curve B). The curve A includes the $T_c(P_{pl})$ for YC1236 without CuO chain and $\text{Y}_{0.8}\text{Ca}_{0.2}\text{Ba}_2\text{Cu}_3\text{O}_y$ with $y < 6.6$. Further, the $T_c(P_{pl})$ for CLBCO and C_xLBLCO without ordered chain also follows the curve A.^{16,26} In the curve A, two data for Y123 are included. The samples for these data were prepared over 10 years ago. It is well known that tuning the oxygen-content using the quenching technique often leads to a large degree of in-plane disorder which causes localization and strong T_c suppression.³⁴ The disorder can be removed by low- T annealing, since the low- T annealing causes the oxygen-rearrangement forming CuO chains.³⁵ The data from the relative new Y123 samples falls on the curve B. The Y123 data on the curve A may have some disorder within the CuO chain layers, although it does not

have the macroscopic chain ordering. Accordingly, the curve A is for the samples with no chain or disordered chain fragments and curve B is for the samples with the relative aligned chain fragment. In $Y_{0.8}Ca_{0.2}Ba_2Cu_3O_y$ with $y \approx 6.5$, the P_{pl} is ~ 0.20 and it shows the tetragonal symmetry.³² The curve B merges into the curve A at $P_{pl} \approx 0.18$. The anisotropy of the in-plane resistivity of the pure $YBa_2Cu_3O_y$ becomes significantly above $y \approx 6.68$ ($P_{pl} \approx 0.18$).² Accordingly, it is considered that until $P_{pl} \sim 0.18$ the superconductivity and TEP are not influenced by the long chain ordering. In spite of the same hole concentration, the T_c for the curve B is slightly higher than that for the curve A. This seems to suggest that the formation of the CuO chain fragment may enhance the coupling between the CuO₂ planes.

D. Comparison with the hole concentration determined by other techniques: the validity of the present scale

The hole concentration can be chemically estimated also from the formal valency of Cu through the titration technique. From the reported S^{290} and the Cu valency for the double-layer $HgBa_2CaCu_2O_{6+\delta}$ (Hg1212) and triple-layer $HgBa_2Ca_2Cu_3O_{8+\delta}$ (Hg1223),^{36,37} the P_{pl} and the hole concentration determined from the Cu valency, P_{CV} are calculated. The P_{CV} of Hg1212 and Hg1223 are plotted into the Fig. 7 as the up- and downward triangle, respectively. In both systems, the P_{CV} is almost identical to P_{pl} . In the overdoped side for the multi-layer HTSC, the inhomogeneity charge distribution for in-equivalent CuO₂ layers was reported.³⁸ We can not address this issue in our data. Also, for an unknown reason, the P_{pl} by TEP does not coincident with P_{CV} for

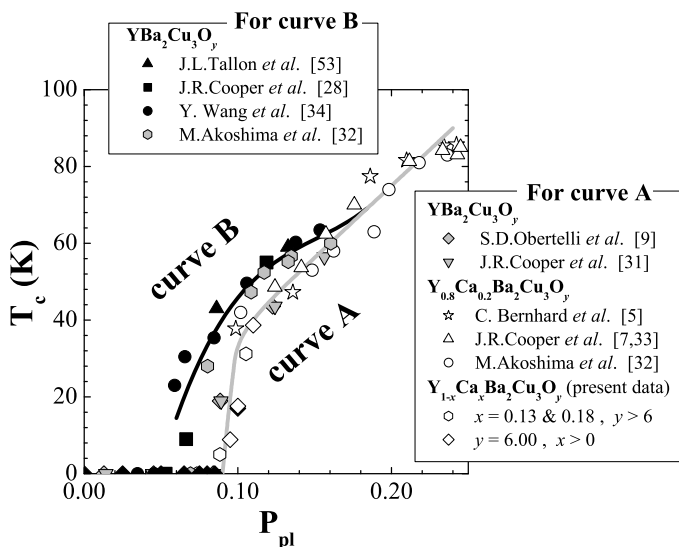


FIG. 6: T_c as a function of P_{pl} in $Y_{1-x}Ca_xBa_2Cu_3O_y$. The solid lines are guide to the eyes.

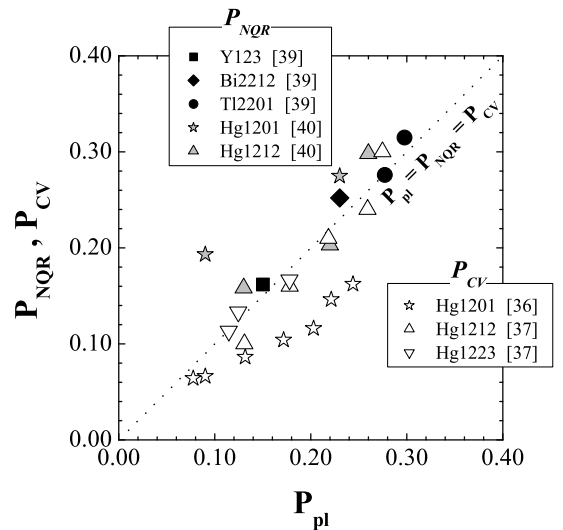


FIG. 7: P_{pl} determined from TEP by the present scale vs P_{NQR} determined from NQR and P_{CV} determined from Cu valency. The solid line shows $P_{pl} = P_{NQR} = P_{CV}$.

the single-layer Hg1201.

The hole concentration for $YBa_2Cu_3O_{6.6}$, $Bi_2Sr_2CaCu_2O_y$ ($T_c = 86$ K) and $Tl_2Ba_2CuO_{6+\delta}$ (Tl2201) with $T_c = 80$ K and 42 K was estimated from the nuclear quadrupole frequency for single- and double-layer HTSC's.³⁹ The reported hole concentration determined from the nuclear quadrupole resonance (NQR), P_{NQR} is plotted into Fig. 7 as a function of the P_{pl} . The broken line exhibits the $P_{pl} = P_{NQR}$ line. The P_{pl} shows a good correlation with P_{NQR} in the wide doped range from 0.15 to 0.3. According to the relation between Knight shift perpendicular to the c-axis and hole concentration for single- and double-layer HTSC's in Ref. 39, we can estimate P_{NQR} for the reported Knight shift data of $HgBa_2CuO_{4+\delta}$ (Hg1201) and Hg1212.⁴⁰ The P_{NQR} of Hg1201 and Hg1212 are plotted into the same figure as the star and upward triangle, respectively. Although underdoped Hg1201 deviates from the $P_{pl} = P_{NQR}$ line, both samples also show the good correlation. The correspondence between P_{pl} and P_{NQR} is suggests that the macroscopic hole concentration determined from TEP is consistent with the microscopic hole concentration determined from NQR.

E. Electronic phase diagram by RT scale

We try to validate our scale by examining the pseudogap behavior in various HTSC's. Since the pseudogap state found in $\rho,^2$ ARPES,⁴ and nuclear magnetic resonance (NMR) experiments⁴¹ has emerged as an intrinsic property of the electronic states of underdoped HTSC, if plotted on a physically meaningful scale, we expect a universal pseudogap behavior for all HTSC's.

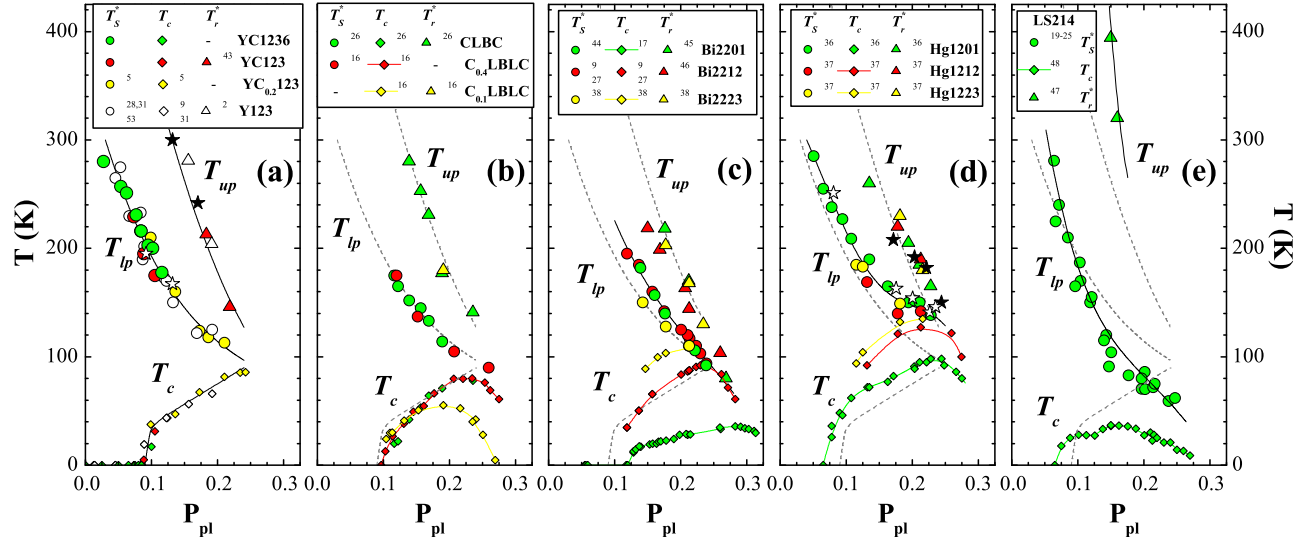


FIG. 8: (color online) T_{up} and T_{lp} vs P_{pl} in (a) Y123 and YC123, (b) CLBC and C_x LBLC (c) Bi-based family, (d) Hg-based family and (e) LS214. All solid lines are guide to the eyes for T_{up} , T_{lp} and T_c . The dashed lines represent the same curves as the solid lines for Y123 and YC123.

Firstly, the phase diagram for $Y_{1-x}Ca_xBa_2Cu_3O_y$ (YC123) and Y123 is shown in Fig. 8(a). T_S^* 's for YC1236, YC123,⁴³ $Y_{0.8}Ca_{0.2}Ba_2Cu_3O_y$ (YC_{0.2}123),⁵ and Y123^{28,31} are found to lie on a common curve which decreases from ~ 300 K at $P_{pl} \approx 0.025$ to ~ 100 K at $P_{pl} \approx 0.24$. T_c 's for YC1236, YC123,⁵ and Y123^{9,31} also lie on a common curve which appears at $P_{pl} \approx 0.09$ and reaches T_c^{max} at $P_{pl} \approx 0.25$. T_S^* seems to be smoothly connected with T_c at slightly overdoped level. T_S^* for both curve A and curve B in Fig. 6 lay on the same $T_S^*(P_{pl})$ curve. Another characteristic temperature T_r^* , where ρ exhibits a downward deviation from the T -linear behavior, for Y123,² and YC123,⁴³ form another curve above the T_S^* curve. Noted that all T_c 's fall on the same curve and therefore, for the same structure, T_c can be used as a secondary measure of P_{pl} if S^{290} is not available. Hereafter, we will call temperatures determined by T_r^* and T_S^* as *upper pseudogap temperature* T_{up} and *lower pseudogap temperature* T_{lp} , respectively. In Fig. 8(b), we plot T_S^* , T_r^* and T_c for CLBC²⁶ and C_x LBLC¹⁶ that have crystal structure similar to that of Y123.¹⁵ They are tetragonal with no ordered chain. T_S^* and T_r^* fall exactly on the T_{lp} and T_{up} curves found in Y123 and YC123, respectively. Same T_{up} and T_{lp} curves can be obtained for Bi-based family of Bi2201,^{17,44,45} Bi2212,^{9,27,46} and Bi₂Sr₂Ca₂Cu₃O_y (Bi2223)³⁸ as shown in Fig. 8(c) and Hg-based family of Hg1201,³⁶ Hg1212,³⁷ and Hg1223³⁷ as shown in Fig. 8(d), respectively. This clearly suggests that *two pseudogaps* do not depend on the number of CuO₂ layers in the unit cell. However, the superconductivity is enhanced with increasing the number of layers, consistent with the empirical rule of T_c for HTSC. The phase diagram for LS214 is shown in Fig. 8(e).^{19,20,21,22,23,24,25,47,48} It is seen that *both pseudogaps*

follow the universal curves until $P_{pl} \approx 0.15$ where the optimal T_c is. It is interesting to note that although our universal P_{pl} scale was originally derived from S^{290} of LS214 it does seem that it is an exceptional member of HTSC as commonly believed.

Here, we further demonstrate the possible application and the advantages of using our scale. In Fig. 9(a), we plot the spin gap temperature signaled by a decrease in ⁶³Cu nuclear relaxation rate ${}^{63}(T_1T)^{-1}$ with reducing T and the pseudogap temperature suggested by the disappearance of leading-edge gap observed by

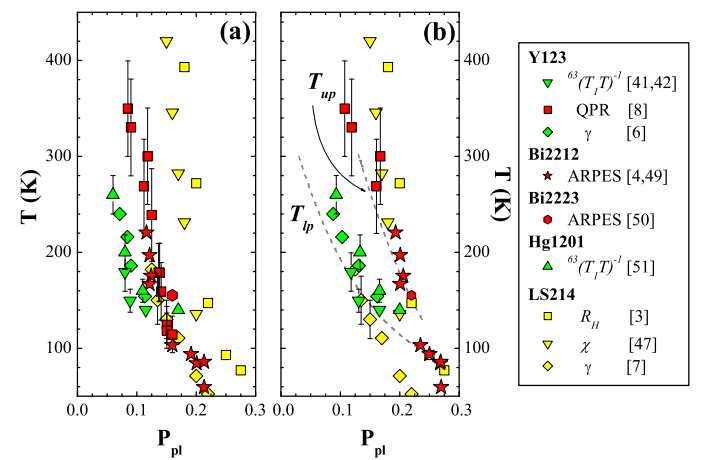


FIG. 9: (Color online) Comparison of various characteristic temperatures determined by different probes for different HTSC's as a function of P_{pl} (a) exactly as reported and (b) using Formula (3). For details see text. The T_{up} and T_{lp} curves (dashed lines) are same as those in Fig. 8.

ARPES as a function of P_{pl} exactly as reported in the literature.^{4,41,49,50,51} There is no clear distinction between them and they seem to behave as one pseudogap. However if we re-plot the same data using our scale,⁵² Fig. 9(b), pseudogap and spin gap clearly belong to the T_{up} and T_{lp} , respectively.

It is interesting to note that the characteristic temperature determined from the time resolved quasiparticle relaxation (QPR) measurement,⁸ R_H ,³ and magnetic susceptibility χ ,⁴⁷ that are also included in Fig. 9, fall on the T_{up} curve. The temperature of a broad peak observed in T -dependnce of the electronic specific heat coefficient γ falls on the T_{lp} curve.^{6,7}

Finally, we would like to point out that T_{lp} and T_{up} are not two different temperatures, determined by different experimental probes, of a common origin. Rather, they have distinct different physical origins. This can be infer from the suppression of $S(T)$ by Zn doping below a certain temperature T_{S2}^* ($>T_S^*$). The T_{S2}^* 's (filled stars) lie exactly on the T_{up} curve as shown in Fig. 8(a) and (d), while T_S^* (open stars) for the samples doped until 1 % in $\text{YBa}_2(\text{Cu}_{1-z}\text{Zn}_z)_3\text{O}_y$ and 3 % in $\text{HgBa}_2(\text{Cu}_{1-z}\text{Zn}_z)\text{O}_{4+\delta}$ fall on the T_{lp} curve.^{36,53} Therefore both T_{lp} and T_{up} are sequentially observed by a single S measurement. This result strongly suggests that there are two characteristic temperatures and they are independent of Zn-doping.

Although there are various discussions for double pseudogaps,^{54,55,56,57,58} our results provide clear experimental evidences that there are indeed *two distinct universal intrinsic* pseudogaps in HTSC. The physical origins of *upper* and *lower pseudogaps* could be attributed to the onset of the electronic inhomogeneity and the superconducting fluctuation, respectively.⁵⁵ If we adopt this scenario, our results indicate that both electronic inhomogeniety and superconducting fluctuation in the pseudogap regime are strictly "2D". Further experimental and theoretical efforts are required to pin down

the physical origins of these two pseudogaps.

IV. SUMMARY AND CONCLUSIONS

In summary, we have shown that $S^{290}(P_{pl})$ of the double-layer $\text{Y}_{1-x}\text{Ca}_x\text{Ba}_2\text{Cu}_3\text{O}_6$ follows that of the single-layer LS214 and can be represented by Formula (3). Although it is not clear exactly how this scale works so well, we argued that S^{290} represents a measure of an intrinsic equilibrium property of the electronic states of doped holes and, therefore, can be used as a common scale to measure P_{pl} of layered HTSC cuprates. Indeed, S^{290} 's were found, independent of if it is doped with hard or soft dopants,⁵⁹ to be identical in both $\text{La}_2\text{CuO}_{4+\delta}$ and $\text{La}_{2-z}\text{Sr}_z\text{CuO}_4$ up to $P_{pl} \approx 0.1$.⁶⁰ A universal phase diagram for HTSC is constructed by using our proposed scale of S^{290} . We conclude that there are *two pseudogaps* and *both pseudogaps* are intrinsically a single CuO_2 layer, therefore 2D in nature, property and T_c depends on the inter-layer coupling for all HTSC's. Our proposed scale points to a unified way to systematically study and compare physical properties of different HTSC and provides further insights of the possible distinct origins of *two pseudogaps*.

Acknowledgments

T.H. would like to thank Dr. K. Yamaya, Dr. K. Kodaira and Dr. S. Yomo for supporting the present research at the initial stage. We are indebted to Dr. Y.S. Song for his technical assistance with S measurement. This work was supported by the state of Texas through the Texas Center for Superconductivity at the University of Houston.

* E-mail address : homma@asahikawa-med.ac.jp

- ¹ H. Yasuoka, T. Imai and T. Shimizu, in *Strong Correlations and Superconductivity*, edited by H. Fukuyama, S. Maekawa, A.P. Malozemoff, Springer Series in Solid-State Sciences, Vol.89 (Springer-Verlag, Berlin, 1989), p. 254.
- ² T. Ito, K. Takenaka, S. Uchida, Phys. Rev. Lett. **70**, 3995 (1993).
- ³ H. Hwang *et al.*, Phys. Rev. Lett. **72**, 2636 (1994).
- ⁴ H. Ding *et al.*, Nature (London) **382**, 51 (1996).
- ⁵ C. Bernhard and J.L. Tallon, Phys. Rev. B **54**, 10201 (1996).
- ⁶ J.W. Loram, K.A. Mirza, J.R. Cooper and W.Y. Liang, Phys. Rev. Lett. **71**, 1740 (1993).
- ⁷ J.W. Loram *et al.*, J. Phys. Chem. Solids **59**, 2091 (1998).
- ⁸ V.V. Kabanov, J. Demsar, B. Podobnik and D. Mihailovic, Phys. Rev. B **59**, 1497 (1999).
- ⁹ S.D. Obertelli, J.R. Cooper and J.L. Tallon, Phys. Rev. B **46**, 14928 (1992).
- ¹⁰ J.L. Tallon and J.W. Loram, Physica (Amsterdam) **349C**, 53 (2001).
- ¹¹ M.R. Presland *et al.*, Physica (Amsterdam) **176C**, 95 (1991).
- ¹² J.L. Tallon, Physica (Amsterdam) **168C**, 85 (1990).
- ¹³ J.L. Tallon *et al.*, Phys. Rev. B **51**, 12911 (1995).
- ¹⁴ R.S. Markiewicz and C. Kusko, Phys. Rev. B **65**, 064520 (2002).
- ¹⁵ D. Goldschmidt *et al.*, Phys. Rev. B **48**, 532 (1993).
- ¹⁶ A. Knizhnik *et al.*, Physica (Amsterdam) **321C**, 199 (1999).
- ¹⁷ Y. Ando *et al.*, Phys. Rev. B **61**, 14956 (2000).
- ¹⁸ E.S. Choi, J.S. Brooks, J.S. Qualls and Y.S. Song, Rev. Sci. Instrum. **72**, 2392 (2001).
- ¹⁹ Y. Nakamura and S. Uchida, Phys. Rev. B **47**, 8369 (1993).
- ²⁰ T. Nishikawa, J. Takeda and M. Sato, J. Phys. Soc. Jpn. **63**, 1441 (1994).
- ²¹ J.-S. Zhou and J.B. Goodenough, Phys. Rev. B **51**, 3104 (1995).
- ²² N. Kakinuma, Y. Ono and Y. Koike, Phys. Rev. B **59**, 1491 (1999).

²³ D.C. Johnston *et al.*, Phys. Rev. B **36**, 4007 (1987).

²⁴ Z.A. Xu *et al.*, Physica (Amsterdam) **341-348C**, 1711 (2000).

²⁵ Y. Hongjie *et al.*, Physica (Amsterdam) **353C**, 221 (2001).

²⁶ K. Hayashi *et al.*, Czech. J. Phys. **46** (S2), 1171 (1996).

²⁷ M. Akoshima, T. Noji, Y. Ono and Y. Koike, Phys. Rev. B **57**, 7491 (1998).

²⁸ J.R. Cooper and J.W. Loram, J. Phys. I France **6**, 3653 (1998).

²⁹ We exclude compounds with conducting channels other than CuO₂ layer such as chain layer in fully oxygenated YBa₂Cu₃O₇.

³⁰ T. Honma, K. Yamaya, N. Môri and M. Tanimoto, in *Proceeding of the 9th International Symposium on Superconductivity, Sapporo*, 1996, edited by S. Nakajima and M. Murakami (Springer, Tokyo, 1997), p. 253.

³¹ J.R. Cooper, S.D. Obertelli, A. Carrington and J.W. Loram, Phys. Rev. B **44**, 12086 (1991).

³² M. Akoshima and Y. Koike, J. Phys. Soc. Jpn. **67**, 3653 (1998).

³³ J.R. Cooper *et al.*, Physica (Amsterdam) **341-348C**, 855 (2000).

³⁴ Y. Wang and N.P. Ong, cond-mat/0110215v1 (2001).

³⁵ B.W. Veal *et al.*, Phys. Rev. B **42**, 4770 (1990).

³⁶ A. Yamamoto *et al.*, Phys. Rev. B **65**, 104505 (2002).

³⁷ A. Fukuoka *et al.*, Phys. Rev. B **55**, 6612 (1997).

³⁸ T. Fujii, I. Terasaki, T. Watanabe and A Matsuda, Phys. Rev. B **66**, 024507 (2002).

³⁹ Y. Tokunaga *et al.*, J. Low. Temp. Phys. **117**, 473 (1999).

⁴⁰ Y. Itoh *et al.*, J. Phys. Soc. Jpn. **67**, 312 (1998).

⁴¹ M. Takigawa *et al.*, Phys. Rev. B **43**, 247, (1991).

⁴² A. Goto, H. Yasuoka and Y. Ueda, J. Phys. Soc. Jpn. **65**, 3043 (1996).

⁴³ T. Honma, K. Yamaya, N. Môri and M. Tanimoto, Solid State Commun. **98**, 395 (1996).

⁴⁴ Y. Dumont, C. Ayache and G. Collin, Phys. Rev. B **62**, 622 (2000).

⁴⁵ Y. Ando and T. Murayama, Phys. Rev. B **60**, 6991 (1999).

⁴⁶ M. Oda *et al.*, Physica (Amsterdam) **281C**, 135 (1997).

⁴⁷ T. Nakano *et al.*, Phys. Rev. B **49**, 16000 (1994).

⁴⁸ P.G. Radaelli *et al.*, Phys. Rev. B **49**, 4163 (1994).

⁴⁹ J.C. Campuzano *et al.*, Phys. Rev. Lett. **83**, 3709 (1999).

⁵⁰ T. Sato *et al.*, Phys. Rev. Lett. **89**, 067005 (2002).

⁵¹ Y. Itoh *et al.*, J. Phys. Soc. Jpn. **65**, 3751 (1996).

⁵² Since there is no corresponding S^{290} data except LS214, P_{pl} of all data points plotted in Fig. 4(b) were determined by " T_c ", our secondary measure of P_{pl} .

⁵³ J.L. Tallon *et al.*, Phys. Rev. Lett. **75**, 4114 (1995).

⁵⁴ B. Batlogg and V.J. Emery, Nature (London) **382**, 20 (1996).

⁵⁵ V.J. Emery, S.A. Kivelson and O. Zachar, Phys. Rev. B **56**, 6120 (1997).

⁵⁶ J. Schmalian, D. Pines and B. Stojković, Phys. Rev. Lett. **80**, 3839 (1998).

⁵⁷ R.S. Markiewicz, Phys. Rev. Lett. **89**, 229703 (2002).

⁵⁸ D. Mihailovic, V.V. Kabanov, K. Žagar and J. Demsar, Phys. Rev. B **60**, 6995 (1999).

⁵⁹ B. Lorenz, Z.G. Li, T. Honma and P.H. Hor, Phys. Rev. B **65**, 144522 (2002).

⁶⁰ Z.G. Li *et al.*, Phys. Rev. Lett. **77**, 5413 (1996).